Desalination and Water Treatment
www.deswater.com

doi: 10.1080/19443994.2016.1180481

57 (2016) 23097–23109
October

Taylor & Francis
Taylor & Francis Group

Experimental parametric analysis of a solar pilot-scale multi-effect distillation plant

Patricia Palenzuela*, Diego C. Alarcón-Padilla, Guillermo Zaragoza

CIEMAT-Plataforma Solar de Almería, Ctra. de Senés s/n, 04200 Tabernas, Almería, Spain, Tel. +34 950387800, ext. 909; Fax: +34 950365015; email: patricia.palenzuela@psa.es (P. Palenzuela)

Received 21 May 2015; Accepted 3 March 2016

ABSTRACT

A 72 m^3/d pilot low-temperature multi-effect distillation plant located at the Plataforma Solar de Almería has been experimentally characterized at steady state to study the influence of the variation in certain parameters that control the process (the hot water inlet temperature as external thermal energy source and the last effect vapor temperature) on the distillate production, the thermal consumption, and the thermal energy efficiency of the plant. Results allowed characterizing the increase in the water production and the thermal consumption with the increase in the hot water inlet temperature and with the decrease in the last effect vapor temperature. The performance ratio reached its maximum when the last effect vapor temperature ranged from 25 to 35°C, since the temperature difference between effects was lower. The preliminary characterization of this plant provides useful experimental information for design criteria and for the analysis of control strategies of other large-scale MED plants and its coupling with solar energy, as well as for identifying some operation issues of the MED technology.

Keywords: Desalination; Multi-effect distillation; Experimental analysis

1. Introduction

Desalination technologies that make use of low-grade thermal energy are proposed to be combined with solar energy technologies to mitigate the water deficit [1,2]. This combination could result also attractive in places where fossil fuel resources are not a limiting factor, since it can help to conserve such resources as well as to reduce the carbon footprint of desalination [3]. The most used desalination technology in the world is reverse osmosis (RO), which is powered by electrical energy. The combination of RO with photovoltaics is limited by the high cost of batteries to guarantee the constant operation required for RO and nowadays, the simpler and more cost-effective means for storing energy are those ones used in the solar thermal technologies.

Regarding thermal desalination technologies, multi-effect distillation (MED) has high overall efficiency, high heat transfer coefficient, and less water recycling in comparison to multi-stage flash [4–6]. As a matter of fact, MED is gaining market share and, in the future, the trend toward MED may be reinforced by

*Corresponding author.

Presented at EuroMed 2015: Desalination for Clean Water and Energy Palermo, Italy, 10–14 May 2015. Organized by the European Desalination Society.

its greater compatibility with solar thermal desalination [7], especially in the case of multi-effect stack (MES) configurations [8]. On the other hand, models predict that the combination of CSP with MED can be more efficient than with RO in the Arabian Gulf region [9]. Moreover, MED has a market niche for solar desalination in the case of medium-scale productions owing to the following advantages: lower energy consumption, compactness, high product quality, and reduced pre-treatment [10]. Even more, this technology is suitable for other applications in which RO has operational limitations (e.g. for desalination of water with high salinity or industrial wastewaters). In order for MED to increase its market share, a reduction in energy consumption and costs would be required. Also, there is a need to select the best combinations for coupling MED with solar energy in order to make this combination a viable option in remote locations. This selection is mainly dependent on the site, although other factors as availability of land, the land cost, and the availability of technical staff should be also taken into consideration [11].

Although the experimental parametric analyses can provide a useful reference for the design, optimization, and development of control strategies with other MED plants, especially relevant in the case of solar desalination plants, most of works found in the literature are based on theoretical analyses from modeling of MED systems. El-Dessouky et al. [12–14], Darwish et al. [15,16], and Aly and El-Fiqi [17] proposed steady state mathematical models for design and analysis of MED plants with forward feed (FF) arrangement. Mistry et al. [18] also presented a steady state model for a FF-MED unit and they compared the results of their model with other published in the literature using parametric analyses. Druetta et al. [19] analyzed and optimized a MED system using a steady state model. Leblanc et al. [20] implemented the model of a MED pilot plant fed by hot water from a solar pond, which was used for the plant design. The model was validated with experimental results with a good agreement. Palenzuela et al. [21,22] developed a steady state model for a vertically stacked FF-MED pilot plant located at Plataforma Solar de Almería. The model was validated with data from the pilot plant showing relative errors lower than 9%. El-Nashar and Qamhiyeh [23] developed a dynamic model, particularized for a vertically stacked MED plant located at Abu Dhabi (UAE) with the aim of studying the transient operation of the plant. The model was validated using the data collected from one start-up period of the plant, showing that it could predict the transient behavior with a reasonable accuracy. Dardour et al. [24] and Ge et al. [25] presented dynamic models of MED plants coupled to nuclear reactors to simulate their dynamic behavior. In the case of the work presented by Roca et al. [26] and De la Calle et al. [27], the dynamic model was based on solar MED plants and the models were validated against actual data from the MED plant located at Plataforma Solar de Almería (Almeria, Spain). Few papers show results of pilot-scale practical experiences. Qi et al. [28] carried out an experimental campaign of a pilot MED system installed in Tianjin (China) to study the effects of several parameters (motive steam pressure, maximum operating temperature, temperature difference, spray density, and steam extraction flow) on the desalination performance. Shahzad et al. [29] presented the results obtained from experiments performed in a three-stage MED coupled to an adsorption cycle in order to prove the increase in the distillate production comparing with a conventional MED plant. Joo and Kwak [30] carried out the design and manufacture of a 3 m^3/d capacity driven by solar energy and evaluated the performance of this unit under different operating conditions. Tigrine et al. [31] presented the experimental results of a MED laboratory prototype, designed in the Development Unit of Solar Equipment UDES (Algeria), that can be connected in the future with a solar heating system. The test campaign was focused on the study of the influence of some parameters of the plant on the distillation yield. Yang et al. [32] presented the design of a fossil five-effect distillation experimental unit and the experimental results in terms of distillate production and Gain Output Ratio were shown. Finally, Georgiou et al. [33] evaluated experimentally the performance of a pilot MED with plate heat exchangers and the potential of its integration with a concentrated solar power system.

The solar desalination unit located at the PSA is a high-efficient solar MES plant, fully monitored, which makes it the perfect vessel for research on improvements of the technology. This work presents a steady state experimental parametric analysis of the plant as a function of two of the operating variables. The analysis of the dynamics of the MED has not been addressed, so the present research work does not account for the transients of the plant against disturbance of the variables of the system. Instead, this approach allows studying the influence of the variation of the hot water inlet temperature (e.g. solar field could work at a lower temperature during winter in order to extend its operation time) and the MED last effect vapor temperature (seasonal variation in seawater temperature) on the thermal performance, the thermal consumption and the distillate production of the plant. The operating variables were varied in a wide operational range: last effect vapor temperature

between 25 and 35˚C and the hot water inlet temperature between 65 and 75˚C. The results of the characterization and a description of the operational issues of the pilot plant are presented.

2. Experimental system

The MED plant located at the Plataforma Solar de Almería, MED-PSA, was manufactured and delivered by ENTROPIE in 1987. In the original experimental desalination system, the first effect worked with saturated vapor at 70˚C (0.312 bar a) generated from a parabolic trough solar field [34]. In 2005, some modifications were carried out at the plant under the framework of the European project AQUASOL (March 2002–February 2006), among others, the first effect of the plant was changed to work with hot water from a static collector solar field and a double-effect absorption heat pump (DEAHP) was installed to be alternatively coupled to the MED plant [35–38]. Fig. 1 shows the layout of all the components of the AQUASOL experimental facility. As seen in the figure, the MED plant can operate with hot water from a solar field composed of static compound parabolic solar collectors (CPC) in the low-temperature operation mode, or with hot water from a double-effect absorption heat pump, DEAHP (LiBr-H_2O). The whole test campaign presented in this paper was carried out only with hot water from the CPC solar field. In this case, the water from the secondary tank is heated while flowing through the solar field going afterward to the primary tank. Then, the hot water from this tank enters the first effect of the MED-PSA plant. The solar field is composed of 252 static CPC collectors with a concentration factor of 1.12 (Fig. 2(a)), an aperture area of 500 m^2 organized in four rows (titled = 35˚) with 63 collectors each one. On the other hand, the storage system is composed of two interconnected tanks of 12 m^3 capacity each (Fig. 2(b)), that store the excess of thermal energy supplied by the solar field and provide the hot water temperature required by the MED plant by the valve V2 (Fig. 1).

The MED-PSA is a forward-feed MED with 14 cells in a vertical arrangement (Fig. 3) at decreasing pressures and temperatures from the 1st cell (on the top) to the 14th one. The exact configuration of the plant is shown in Fig. 4, where all the streams corresponding to brine, steam, distillate and hot water are represented. The design and operating parameters are shown in Table 1 (note that the operating parameters correspond to those under nominal conditions). The design parameters are: the number of effects,

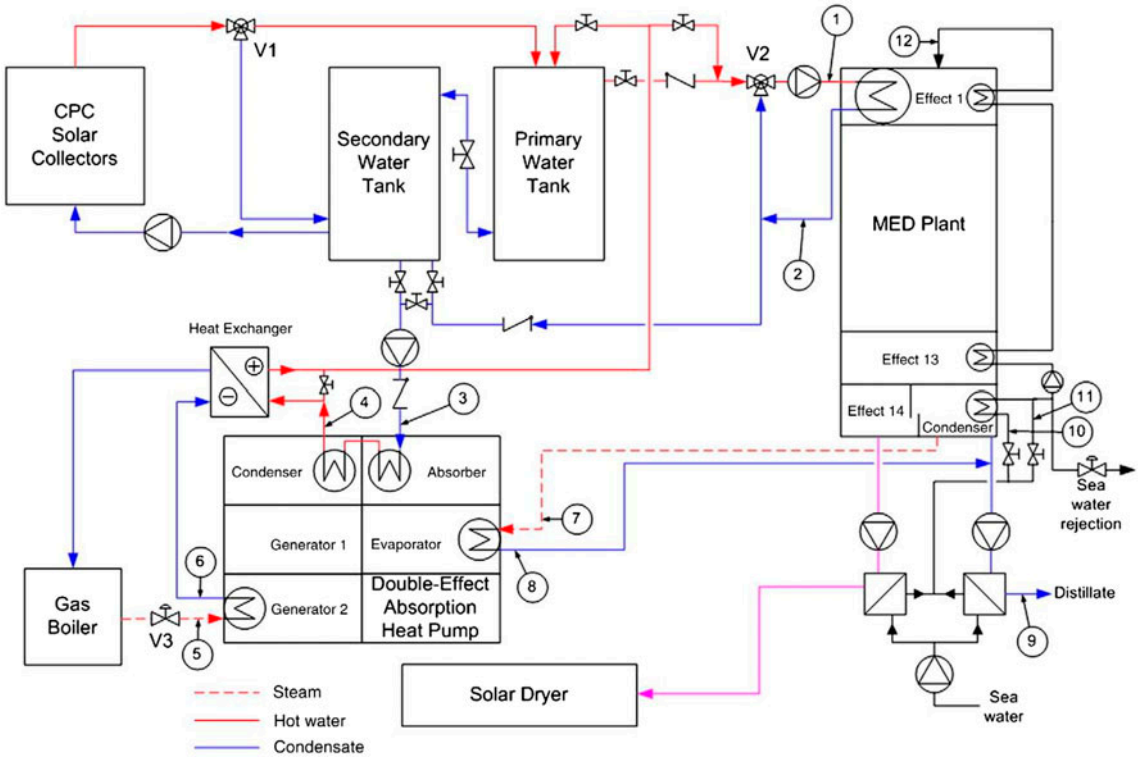

Fig. 1. Layout of the AQUASOL system.

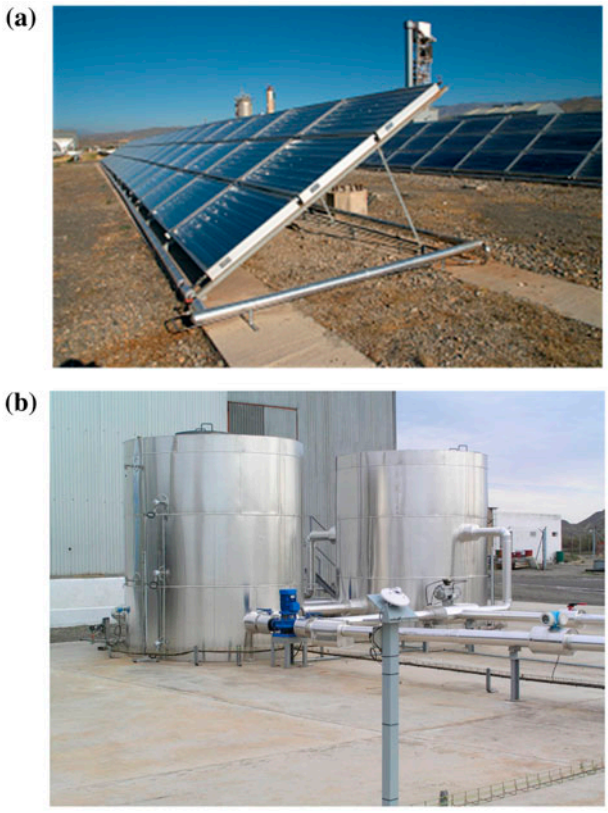

Fig. 2. CPCs collectors' solar field (a) and thermal storage tanks (b) installed at PSA.

the number of preheaters, the top brine temperature, the temperature increase through the condenser (temperature difference between inlet and outlet seawater cooling stream), the inlet seawater temperature, the conversion ratio, the distillate production and the inlet/outlet hot water temperatures. The operating parameters are: the feedwater flow rate, the total brine production, the cooling seawater flow rate, the vapor production at the last effect, the Performance Ratio, the hot water flow rate, and the thermal consumption.

Apart from the first and the last cell, the remaining ones are identical. Each cell is composed of two horizontal tube bundles, called evaporator and preheater. The preheater located in the last cell (called final condenser) is much bigger than the rest since it condenses the entire vapor generated in the last effect. A large volume of seawater is pumped through such condenser, part of this seawater is rejected and the remaining (40% under nominal conditions) is used to feed the plant (called feedwater). The feedwater then flows through the tube bundle of each preheater from the bottom to the top being preheated until reaching the first effect at a temperature close to the evaporation temperature. Here, the feedwater is sprayed over

Fig. 3. MED pilot plant located at the Plataforma Solar de Almería.

the tube bundle of the first evaporator through which the hot water is flowing transferring heat. Part of the feedwater evaporates in the effect and the remaining part, with higher salt concentration, falls over the next effect. The vapor produced in the evaporator flows to the preheater going through a demister that avoids brine droplets in the vapor. Once in the preheater, a small part of the vapor is condensed. The distillate produced and the vapor, which has not been condensed, flow to inside the tube bundle of the next evaporator over which the high concentrated feedwater coming from the first effect is being sprayed. The mixture of distillate and vapor transfer heat to the feedwater producing on one hand vapor from this feedwater and on the other hand distillate from the previous vapor. The same process than before is repeated so on for the rest of effects.

The total plant distillate production consists of the vapor condensed in each effect and in the preheaters plus the distillate generated in the final condenser. As an energy optimization strategy, the distillate produced goes to other effects instead of being extracted from each one in order to recover its sensible heat, which contributes to improve the brine evaporation generating more amount of vapor without increasing the external heat source. The distillate flows to the next effect with the exception of the 4th, 7th, 10th, and

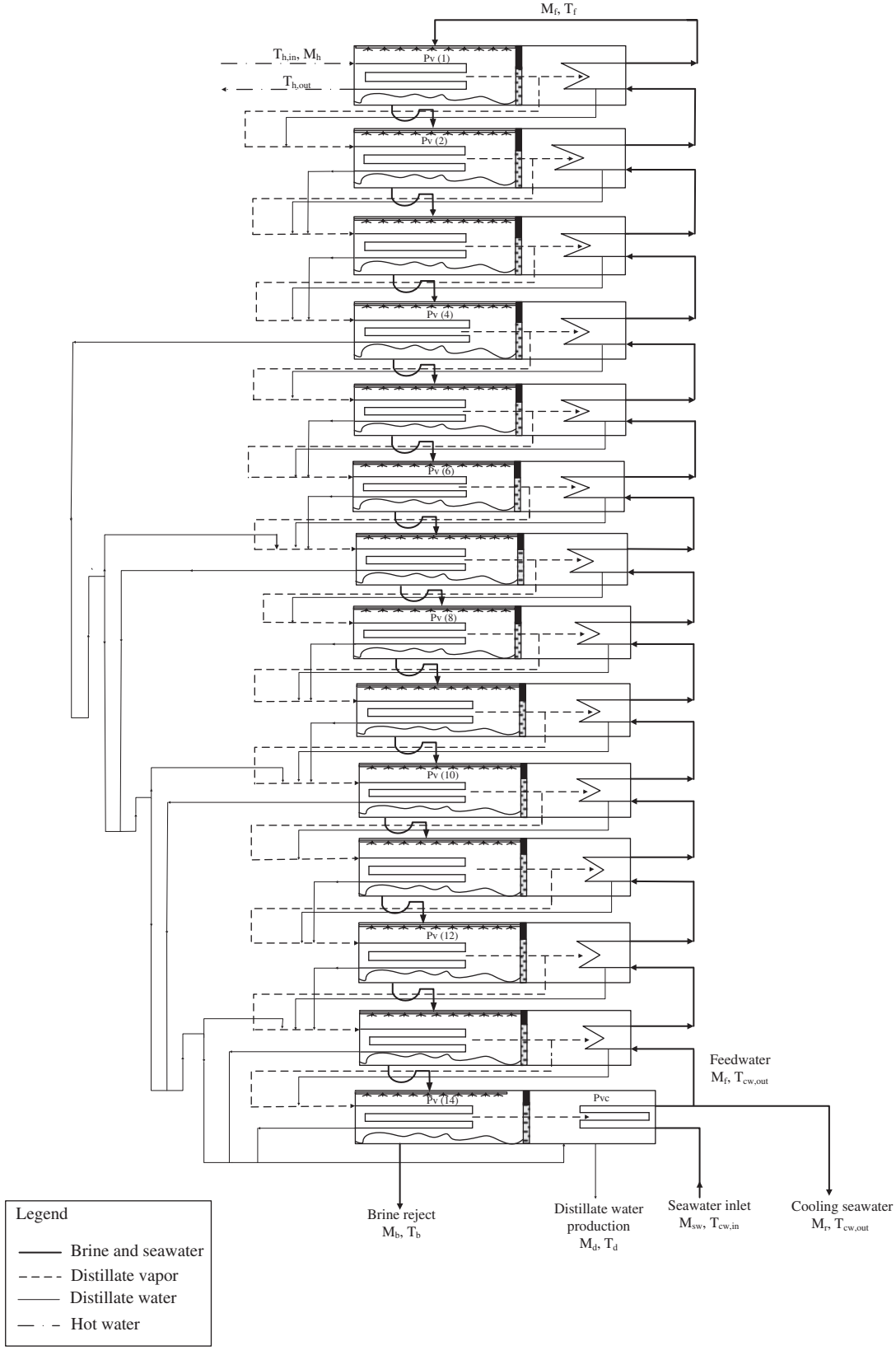

Fig. 4. Schematic diagram of MED plant at the Plataforma Solar de Almería.

Table 1
Design and operating parameters of the MED-PSA plant

Number of effects	14
Number of preheaters	13
Top brine temperature (℃)	70
Temperature increase through the condenser (℃)	10
Inlet seawater temperature (℃)	25
Conversion ratio (%)	37.5
Inlet/outlet hot water temperature (℃)	75/71
Feedwater flow rate (m^3/h)	8
Total brine production (m^3/h)	5
Hot water flow rate (L/s)	12
Total distillate production (m^3/d)	72
Cooling seawater flow rate 25℃ (m^3/h)	20
Vapor production in the last effect (kg/h)	159
Thermal energy consumption in the first effect (kW)	200
Performance ratio	>9

13th cells (as shown in Fig. 4) in order to balance the amount of distillate entering the effects without flooding the bundle tube so as not to make the heat transfer worse.

MED-PSA plant is operated in a closed circuit consisting of two ponds interconnected by a cooling tower: the total distillate produced and the brine rejected are mixed in the small pond and the seawater for the supply of the plant is taken from the bigger one. The rejected cooling seawater from the final condenser is also returned to the small pond and part of the heat released at the condenser could increase its temperature during an experiment. To avoid that, the cooling tower is switched on to cool the water from the small pond before sending it back to the bigger one.

The MED-PSA plant has a vacuum system in order to eliminate the air leakages and the non-condensable gases generated during the desalination process. It consists of two hydro-ejectors, which are connected to effects 2, 7, and the final condenser. They are connected within a closed circuit with a tank and an electric pump that circulates seawater through the ejectors at a pressure of 3 bar.

The pilot plant is experimental and therefore equipped with a comprehensive monitoring system, which provides instantaneous values of the measured data. All the monitored variables are indicated in Fig. 4 and described in the nomenclature.

3. Test campaign

The test campaign aimed to study the influence of the variation in certain operating parameters of the MED plant, like the hot water inlet temperature ($T_{h,in}$) and the MED last effect vapor temperature ($T_v(N)$, on the thermal performance and on the distillate production of the plant. For this purpose, a steady state experimental parametric analysis was performed in the pilot MED plant, keeping the rest of variables that control the process constant and equal to their nominal values and studying the behavior of the plant once steady state conditions are achieved.

Experiments were run during 10 months and were designed following a three-level factorial experimental design (3^k) in which the varying parameters and their three operation levels (−1, 0, and +1) are the ones shown in Table 2. Note that the measured variable inside the effects is the vapor pressure (Fig. 4), so the vapor temperature (T_v) is the saturation temperature at the corresponding pressure (P_v). The range of the parameters was established according to some of the design values of the plant. Specifically, it was taken into account the maximum top brine temperature, TBT (which is limited at 70℃ to avoid scaling) and the temperature difference across effects (between 2.0 and 3.0℃) together to the number of effects ($N = 14$) of this pilot MED plant. Also, it was considered a fixed temperature difference in the condenser between inlet and outlet seawater cooling stream equal to the design value (10℃). Therefore, the different vapor temperatures of the last effect would represent

Table 2
Variable factors and their actual values of operation

	−1	0	+1
Last effect vapor temperature $T_v(N)$ (℃)	25	30	35
Hot water inlet temperature $T_{h,in}$ (℃)	65	70	75

different seawater temperatures at the inlet of the condenser, which is representative of seasonal variations or different locations of the MED plant. Due to the mentioned water supply system of this pilot plant, the temperature at the inlet of the condenser can be controlled by the refrigeration tower to simulate the seawater temperature variations. Because of the limitations in the refrigeration tower due to the ambient temperature, the experiments at the lowest level of operation in the last effect vapor temperature ($T_v(N)$ = 25°C) were carried out during winter months and those at the highest level ($T_v(N)$ = 35°C) during summer months.

Each test lasted an average of 2 or 3 h. The solar radiation available and the thermal energy stored allow the operation of the plant during this period. The stability of the plant is achieved by different control systems, the main one being a PID implemented in valve V2 (Fig. 2) that allows a constant hot water temperature (and at the desirable value) at the inlet of the MED first effect. The operation routine was always the following. Firstly, the vacuum of the plant was made to release the air from the system and the seawater was pumped to the condenser controlling the inlet temperature by switching on the refrigeration tower if necessary. Once all the pressures in the effects and the seawater were stabilized, the corresponding feedwater flow rate was pumped to the first effect of the plant and the hot water was pumped from the primary water tank to the first effect of the MED plant. During the operation, the seawater flow rate through the condenser was varied by a manual valve and the cooling tower was switched on/off in order to keep the last effect vapor temperature at the desirable value. Once steady state conditions were achieved (normally after less than one hour of operation), the measurements were taken for a period of half an hour in order to have enough data that provide a representative average. In all the experiments, the hot water flow rate (M_h) and the feedwater flow rate (M_f) were kept constant at the nominal values (see Table 1) using variable speed pumps adjusted by PID control systems.

4. Results and discussion

Fig. 5 depicts the operation of the MED plant in one of the experiments performed during the test campaign ($T_{h,in}$ = 75°C, $T_v(N)$ = 35°C). It shows the distillate production and the thermal energy consumption of the MED plant, and the global solar radiation. It can be observed that the thermal energy consumed by the plant and its production is quite stable despite the variation in the global solar radiation, which is an indication of the robustness of the control systems used (in the feed and hot water pumps and in Valve 2).

A set of results is depicted in Figs. 6–9. They represent the average value of each variable (distillate production, performance ratio, and thermal consumption) in every test. Error bars have been included in each

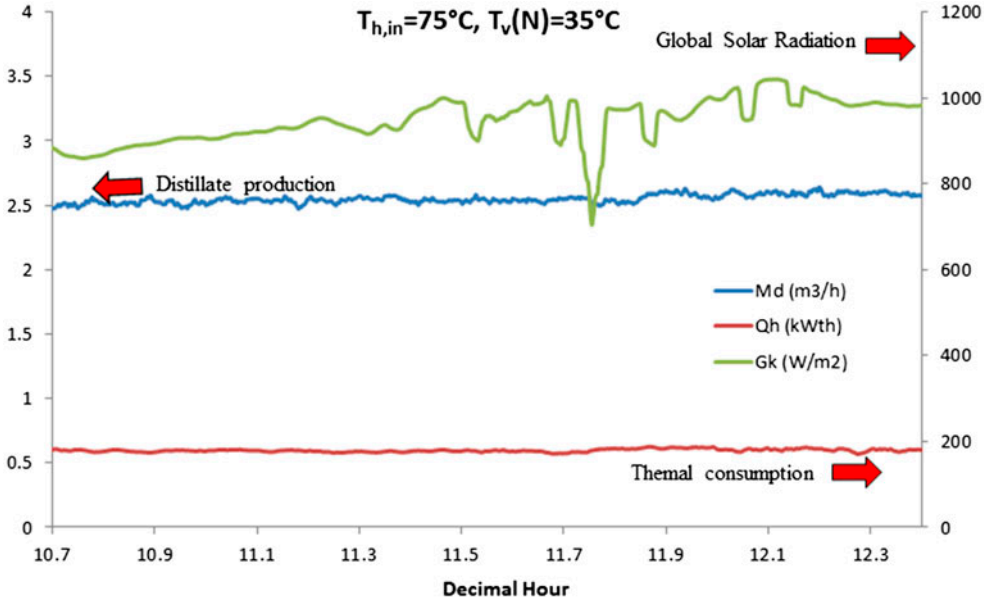

Fig. 5. Distillate production, thermal consumption, and global solar radiation during MED operation at $T_{h,in}$ = 75°C and $T_v(N)$ = 35°C.

figure. In the case of the indirect variables (PR, Q_h, and ΔT_{effect}), an uncertainty propagation analysis has been carried out by the method described in [39]. The measurement uncertainties (U) of the direct variables are: $UT_{h,in}$ = 0.85°C, $UT_{h,out}$ = 0.85°C, UM_h = 0.5%, UP (1) = 3 mbar, UM_d = 0.75%, $UP(N)$ = 1.25 mbar. In the case of ΔT_{effect}, the error bars are not represented in Fig. 9 because the uncertainty resulted insignificant.

Figs. 6 and 7 show the influence of the variation in the last effect vapor temperature and the hot water inlet temperature on the distillate production (M_d) and on the thermal consumption, Q_h (it is determined by Eq. (1)), respectively. As it was found in other published works [40,41], the distillate production increased with the increase in the hot water inlet temperature. It increased by 8–20% when $T_{h,in}$ increased 10°C. The highest rise (20%) was observed when last effect vapor temperature was kept at 35°C:

$$Q_h = M_h C_p (T_{h,in} - T_{h,out}) \quad (1)$$

where C_p is the specific heat at constant pressure mean temperature between $T_{h,in}$ and $T_{h,out}$, in (kJ/kg°C) and $T_{h,out}$ is the hot water outlet temperature, in (°C). The thermal consumption also increased with the hot water inlet temperature as was already shown in Refs. [29,41],

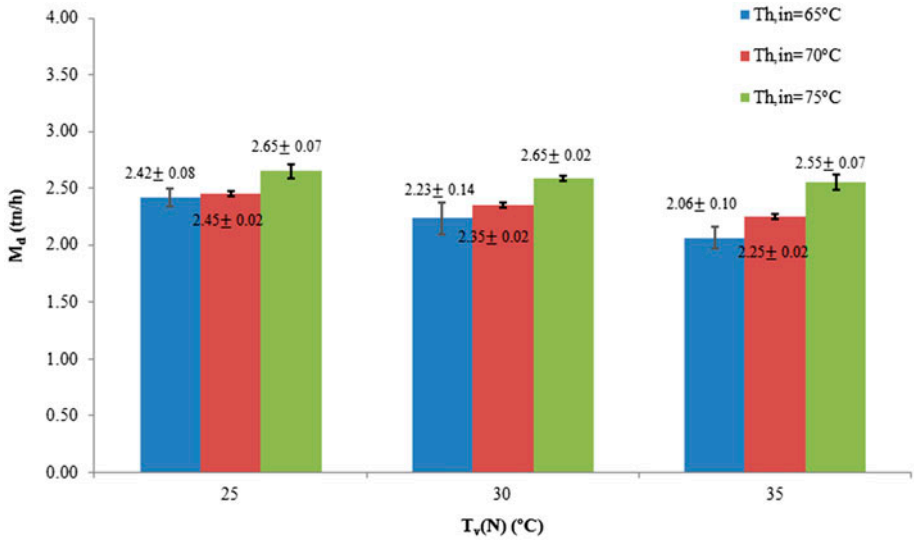

Fig. 6. Influence of the variation in $T_{h,in}$ and $T_v(N)$ on the distillate production (M_h = 12 kg/s, M_f = 8 m^3/h).

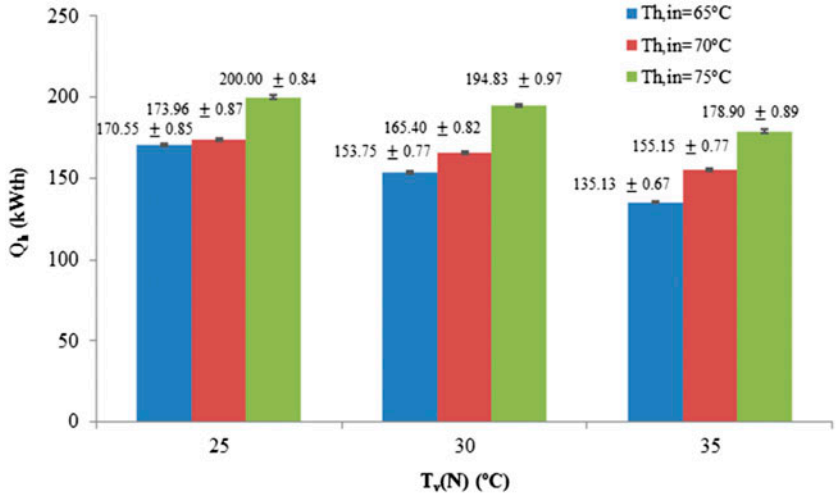

Fig. 7. Influence of the variation in $T_{h,in}$ and $T_v(N)$ on the thermal consumption for M_h = 12 kg/s and M_f = 8 m^3/h.

Table 3
Average values of the overall heat transfer coefficient of the first evaporator for different hot water inlet temperatures keeping the last effect vapor temperature at 35°C

$T_{h,in}$ (°C)	U_h (kW/m^2°C)
65	2.22
70	2.25
75	2.48

showing a rise between 15 and 25% with $T_{h,in}$, being the maximum increase in summer months ($T_v(N)$ = 35°C). The increase in M_d is caused by a rise in the rate of vapor formation inside the first effect. As a consequence, a higher amount of vapor through the remaining effects is generated increasing the total distillate production of the plant. Likewise, the rise in the vapor formation inside the first effect can be explained by the increase in the overall heat transfer coefficient of the horizontal falling film tube bundle of such effect (U_h), as mentioned in [28]. As observed in Table 3, U_h was enhanced 10% when $T_{h,in}$ was raised from 65 to 75°C. This coefficient was determined by an empirical correlation obtained by the authors of this paper and presented in [24]:

$$\begin{aligned} U_h = {} & 25.1217 - (0.0992825 \cdot T_v(N)) - (0.678212 \cdot T_{h,in}) \\ & + (0.30056 \cdot M_h) - (0.00323972 \cdot T_v^2(N)) \\ & + (0.00392379 \cdot T_{h,in}^2) - (0.0112135 \cdot M_h^2) \\ & + (0.00442078 \cdot T_v(N) \cdot T_{h,in}) \end{aligned} \quad (2)$$

The increase of U_h in the first effect can be attributed to the decrease in the dynamic viscosity with the boiling temperature in this effect (the dynamic viscosity is lower the higher the temperature), which lead to higher rates of heat transfer [22]. The trend of the overall heat transfer coefficient with the hot water inlet temperature is in agreement with the works published in the literature [12,23,42]. Notice that the minimum difference observed between U_h at 65 and 70°C with respect to the U_h obtained at 75°C can be caused by a better operation of the plant under design conditions (75°C in the hot water inlet temperature) than out of nominal conditions.

On the other hand, Fig. 6 shows that M_d exhibited a downward trend with the increase in the last effect vapor temperature keeping $T_{h,in}$ constant, which is in agreement with other research works [29]. The higher $T_v(N)$ the higher the seawater temperature at the outlet of the condenser ($T_{cw,out}$ in Fig. 4) and therefore at the outlet of the set of preheaters. Consequently, the feedwater reaches the first effect at a higher temperature (T_f in Fig. 4), which decreases the thermal consumption required in the first effect (as shown in Fig. 7). It causes a decrease in the amount of vapor generated in such effect and therefore in that of the vapor generated in the rest of effects, lowering the total distillate production. The fresh water production was higher at lower last effect vapor temperatures ($T_v(N)$ = 25°C) (which is representative of winter months) and the difference with respect to higher last effect vapor temperatures ($T_v(N)$ = 35°C) (representative of summer months) varied between 4 and 15% (this difference was higher the lower the hot water inlet temperature used). On the other side, the desalination process required 21% less of thermal energy (at 65°C) at higher last effect vapor temperature than at lower last effect vapor temperature.

The performance ratio (PR) is defined as the ratio between the mass of distillate (in kg) and the thermal energy supplied to the process normalized to 2,326 kJ (1,000 Btu) that is the latent heat of vaporization of water at 73°C. It is determined by the following equation:

$$PR = \frac{M_d}{Q_h} \times \frac{2326\,\text{kJ}}{1\,\text{kg}} \quad (3)$$

Fig. 8 shows the effect of the hot water inlet temperature and the last effect vapor temperature on the performance ratio. It was observed that *PR* decreased with the increase in $T_{h,in}$, as was found in other published works [13,14,43,44]. It decreased roughly a 7% when $T_{h,in}$ increased from 65 to 75°C. The higher the temperature of the hot water entering the tube bundle of the first effect, the higher the temperature of the vapor generated inside such effect, which increases the temperature lift of the plant (i.e. vapor temperature difference between the first and last effect), keeping the vapor temperature inside the last effect constant. As a matter of fact, the temperature difference across effects, ΔT_{effect} (determined as $T_v(1) - T_v(N)/(N-1)$) increased between 14 and 22% when $T_{h,in}$ was enhanced from 65 to 75°C, respectively (Fig. 9). A rise in ΔT_{effect} results in a decrease of the thermal efficiency of the process due to the fact that the evaporation–condensation process in each effect becomes thermodynamically less reversible (according to the second law of thermodynamics), which causes the decrease in the PR of the plant (and at the same time higher thermal consumptions are required, as seen in Fig. 7). An increase in ΔT_{effect} of 14% resulted in a decrease of 7% in the PR when $T_v(N)$ was 25°C. For $T_v(N)$ 30 and 35°C, the increase in ΔT_{effect} was the double (22%) but it was not observed any variation in the decrease in *PR* (it was kept at roughly 7%). On the

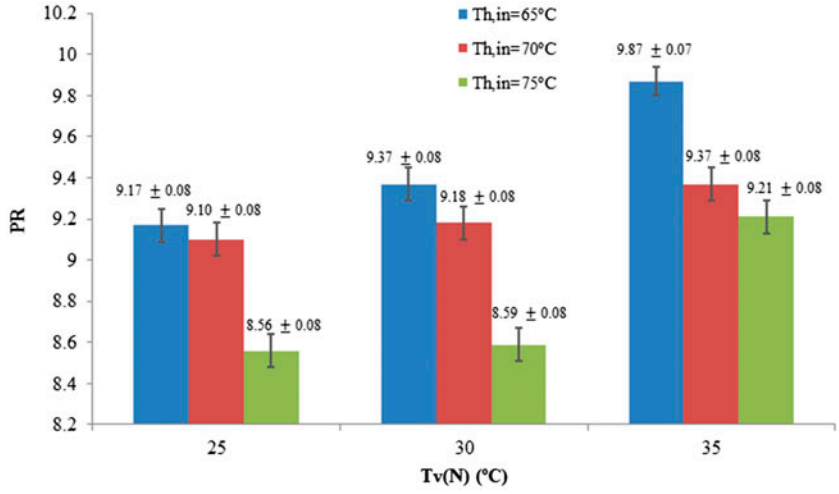

Fig. 8. Influence of the variation in $T_{h,in}$ and $T_v(N)$ on performance ratio (M_h = 12 kg/s, M_f = 8 m^3/h).

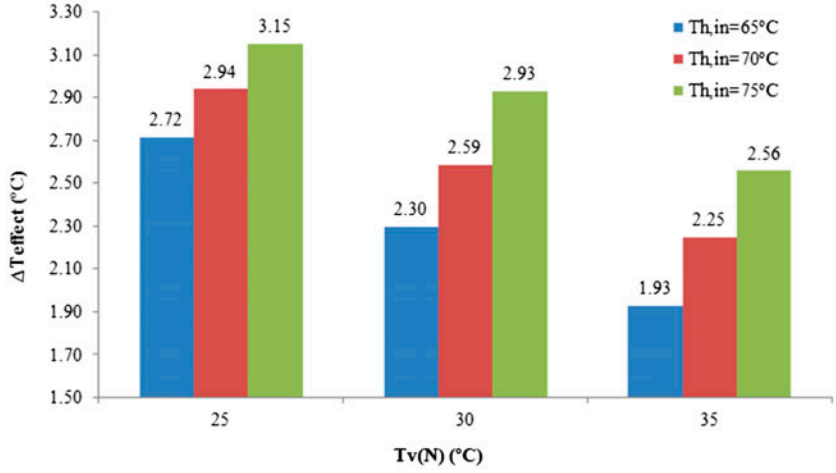

Fig. 9. Variation in ΔT_{effect} with $T_{h,in}$, and $T_v(N)$ (M_h = 12 kg/s, M_f = 8 m^3/h).

other hand, *PR* increased with the increase in $T_v(N)$, which is in agreement with the results found in [28,44]. The higher the last effect vapor temperature, the lower the temperature difference across the effects, when keeping $T_{h,in}$ constant (Fig. 9), which favors the thermal efficiency of the plant, obtaining higher PR (the maximum PR = 9.87 was obtained at $T_v(N)$ = 35°C).

Summarizing, in order to maximize the fresh water production (so to minimize the product costs) and to make the most efficient use of the thermal energy supplied by the solar field to the MED plant, it is recommended to use the following strategies in the operation of the MED coupled to a solar field. During summer months, the seawater temperature is higher and the fresh water demand is also higher, thus the solar field should supply hot water at 70 and 75°C to the desalination plant, keeping $T_v(N)$ at 30 and 35°C, respectively, depending on the solar radiation availability and on the seawater temperature. As has been tested, under these conditions, an increase in the fresh water production up to 20% can be obtained decreasing the *PR* only a 7%. On the contrary, the solar field should be providing hot water at 65 and 70°C to the MED plant during the coldest months, keeping $T_v(N)$ at 25°C (since the seawater temperature is lower). At these operation levels, the solar field would provide thermal energy at a higher efficiency (higher capacity

factor) extending the operation time of the solar MED plant. Also, the plant would produce fresh water with a higher thermal efficiency (2.42 tn/h with a PR of 9.17, and 2.45 tn/h with a PR of 9.10).

5. Conclusions and recommendations

In this paper, a 72 m^3/d low-temperature multi-effect distillation (LT-MED) plant coupled to a compound parabolic solar field was characterized and the effects of key operating parameters were analyzed. The following conclusions can be drawn from the test results:

(1) The tests indicated that water production increased by 8–20% when the hot water inlet temperature increased by 10˚C. The maximum rise in the water production (20%) was obtained for a last effect vapor temperature of 35˚C supplying the hot water at 75˚C.
(2) Thermal consumption decreased with the increase in the last effect vapor temperature, resulting in a 21% less of thermal energy (at 65˚C) when such temperature was 35˚C.
(3) The experiments showed that PR decreased roughly a 7% when the hot water inlet temperature increased from 65 to 75˚C. On the other hand, the PR of the plant increased by 7% keeping the hot water inlet temperature at 65 and 75˚C, and 3% at 70˚C, when the last effect vapor temperature increased 10˚C.
(4) In summer and spring, the MED unit should operate with hot water from the solar field at 70˚C keeping the vapor temperature in the last effect at 30˚C or supplying hot water at 75˚C with 35˚C in the last effect, depending on the solar radiation availability and the seawater temperature.
(5) In winter and autumn, it is recommendable to operate the MED plant with hot water between 65 and 70˚C keeping last effect vapor temperature at 25˚C.

Acknowledgments

The authors wish to thank the European Commission (DG for Research & Innovation) for its financial assistance within the Integrated Research Programme in the field of Concentrated Solar Power (CSP) (STAGE-STE Project; Grant Agreement No. 609837). This work has been also funded by the National R+D+i Plan Project DPI2014-56364-C2-1-R of the Spanish Ministry of Economy and Competitiveness and ERDF funds.

Nomenclature

Variables

$T_v(N)$	—	last effect vapor temperature (˚C)
$T_{h,in}$	—	hot water inlet temperature (˚C)
$T_{h,out}$	—	hot water outlet temperature (˚C)
M_f	—	feedwater feed flow rate (m^3/h)
M_h	—	hot water flow rate (kg/s)
U_h	—	overall heat transfer coefficient (kW/m^2˚C)
M_d	—	distillate production (tn/h)
PR	—	performance ratio
ΔT_{effect}	—	temperature difference across the effects (˚C)
Q_h	—	thermal consumption (kW)
M_b	—	brine flow rate (m^3/h)
T_b	—	brine temperature (˚C)
M_{sw}	—	seawater flow rate entering the condenser (m^3/h)
$T_{cw,in}$	—	seawater temperature at the inlet of the condenser (˚C)
$T_{cw,out}$	—	seawater temperature at the outlet of the condenser (˚C)
T_f	—	feedwater temperature at the outlet of the last preheater (˚C)
T_d	—	distillate temperature (˚C)
P_v	—	vapor pressure inside the effects (mbar)
G_k	—	global solar radiation, (W/m^2)
U	—	uncertainty
	—	

Acronyms and abbreviations

MED	—	multi-effect distillation
LT-MED	—	low-temperature multi-effect distillation
TBT	—	top brine temperature
PSA	—	plataforma Solar de Almería
MSF	—	multi-stage flash
CPC	—	compound parabolic collectors
CSP	—	concentrated solar power
RO	—	reverse osmosis
PF	—	parallel feed

References

[1] K. Soteris, A, Seawater desalination using renewable energy sources, Prog. Energy Combust. Sci. 31 (2005) 242–281.
[2] N. Ghaffour, V.K. Reddy, M. Abu-Arabi, Technology development and application of solar energy in desalination: MEDRC contribution, Renewable Sustainable Energy Rev. 15 (2011) 4410–4415.
[3] J. Lienhard, M. Antar, A. Bilton, J. Blanco, G. Zaragoza, Annual review of heat transfer, Sol. Desalin. 15 (2012) 277–347.
[4] M.A. Darwish, A. Darwish, Solar cogeneration power-desalting plant with assisted fuel, Desalin. Water Treat. 52 (2014) 9–26.
[5] C. Li, Y. Goswami, E. Stefanakos, Solar assisted sea water desalination: A review, Renewable Sustainable Energy Rev. 19 (2013) 136–163.

[6] A. Al-Karaghouli, L.L. Kazmerski, Energy consumption and water production cost of conventional and renewable-energy-powered desalination processes, Renewable Sustainable Energy Rev. 24 (2013) 343–356.
[7] H. Sharon, K.S. Reddy, A review of solar energy driven desalination technologies, Renewable Sustainable Energy Rev. 41 (2015) 1080–1118.
[8] S. Kalogirou, Survey of solar desalination systems and system selection, Energy 22 (1997) 69–81.
[9] P. Palenzuela, D.C. Alarcón, G. Zaragoza, Large-scale solar desalination by combination with CSP: Techno-economic analysis of different options for the Mediterranean Sea and the Arabian Gulf, Desalination 366 (2015) 130–138.
[10] M.A. Eltawil, Z. Zhengming, L. Yuan, A review of renewable energy technologies integrated with desalination systems, Renewable Sustainable Energy Rev. 13 (2009) 2245–2262.
[11] E. Tzen, G. Zaragoza, D.C. Alarcón Padilla, Solar Desalination, in: A. Sayigh (Ed.), Comprehensive Renewable Energy, Elsevier, Oxford, vol. 3, 2012, pp. 529–565.
[12] H. El-Dessouky, I. Alatiqi, S. Bingulac, H. Ettouney, Steady-state analysis of the multiple effect evaporation desalination process, Chem. Eng. Technol. 21 (1998) 437–451.
[13] H.T. El-Dessouky, H.M. Ettouney, Multiple-effect evaporation desalination systems thermal analysis, Desalination 125 (1999) 259–276.
[14] H. El-Dessouky, H. Ettouney, F. Mandani, Performance of parallel feed multiple effect evaporation system for seawater desalination, Appl. Therm. Eng. 20 (2000) 1679–1706.
[15] M.A. Darwish, F. Al-Juwayhel, H.K. Abdulraheim, Multi-effect boiling systems from an energy viewpoint, Desalination 194 (2006) 22–39.
[16] M.A. Darwish, H.K. Abdulrahim, Feed water arrangements in a multi-effect desalting system, Desalination 228 (2008) 30–54.
[17] N.H. Aly, A.K. El-Figi, Thermal performance of seawater desalination systems, Desalination 158 (2003) 127–142.
[18] K.H. Mistry, M.A. Antar, J.H. Lienhard V, An improved model for multiple effect distillation, Desalin. Water Treat. 51 (2013) 807–821.
[19] P. Druetta, P. Aguirre, S. Mussati, Optimization of multi-effect evaporation desalination plants, Desalination 311 (2013) 1–15.
[20] J. Leblanc, J. Andrews, A. Akbarzadeh, Low-temperature solar-thermal multi-effect evaporation desalination systems, Int. J. Energy Res. 34 (2010) 393–403.
[21] P. Palenzuela, A.S. Hassan, G. Zaragoza, D.C. Alarcón-Padilla, Steady state model for multi-effect distillation case study: Plataforma Solar de Almería MED pilot plant, Desalination 337 (2014) 31–42.
[22] P. Palenzuela, D. Alarcón, G. Zaragoza, J. Blanco, M. Ibarra, Parametric equations for the variables of a steady-state model of a multi-effect desalination plant, Desalin. Water Treat. 51 (2013) 1229–1241.
[23] A.M. El-Nashar, A. Qamhiyeh, Simulation of the performance of MES evaporators under unsteady state operating conditions, Desalination 79 (1990) 65–83.
[24] S. Dardour, S. Nisan, F. Charbit, Development of a computer-package for MED plant dynamics, Desalination 182 (2005) 229–237.
[25] Z. Ge, X. Du, L. Yang, Y. Yang, S. Wu, Simulation on the start-up of MED seawater desalination system coupled with nuclear heating reactor, Appl. Therm. Eng. 28 (2008) 203–210.
[26] L. Roca, L.J. Yebra, M. Berenguel, A. de La Calle, Dynamic modeling and simulation of a multi-effect distillation plant, Proceedings of 9th International Modelica Conference, Munich, 2012, pp. 883–888.
[27] A. de la Calle, J. Bonilla, L. Roca, P. Palenzuela, Dynamic modeling and simulation of a solar-assisted multi-effect distillation plant, Desalination 357 (2015) 65–76.
[28] C.H. Qi, H.J. Feng, Q.C. Lv, Y.L. Xing, N. Li, Performance study of a pilot-scale low-temperature multi-effect desalination plant, Appl. Energy 135 (2014) 415–422.
[29] M.W. Shahzad, K. Thu, Y. Kim, K.C. Ng, An experimental investigation on MEDAD hybrid desalination cycle, Appl. Energy 148 (2015) 273–281.
[30] H. Joo, H. Kwak, Performance evaluation of multi-effect distiller for optimized solar thermal desalination, Appl. Therm. Eng. 61 (2013) 491–499.
[31] Z. Tigrine, H. Aburideh, M. Abbas, D. Zioui, R. Bellatreche, N.K. Merzouk, S. Hout, D. Belhout, Experimental investigations on a multi-stage water desalination prototype, Desalin. Water Treat. 56 (2015) 2612–2617.
[32] L. Yang, S. Shen, H. Hu, Thermodynamic performance of a low temperature multi-effect distillation experimental unit with horizontal-tube falling film evaporation, Desalin. Water Treat. 33 (2011) 202–208.
[33] M.C. Georgiou, A.M. Bonanos, J.G. Georgiadis, Experimental evaluation of a multiple-effect distillation unit in low seawater flow conditions, Desalin. Water Treat. 55 (2015) 3267–3276.
[34] A. Gregorzewski, K. Genthner, E. Zarza, J. Leon, The solar thermal desalination research project at the Plataforma Solar de Almería, Desalination 82 (1991) 145–452.
[35] D.C. Alarcón-Padilla, L. García-Rodríguez, Application of absorption heat pumps to multi-effect distillation: A case study of solar desalination, Desalination 212 (2007) 294–302.
[36] D.C. Alarcón-Padilla, L. García-Rodríguez, J. Blanco-Gálvez, Assessment of an absorption heat pump coupled to a multi-effect distillation unit within AQUASOL project, Desalination 212 (2007) 303–310.
[37] D.C. Alarcón-Padilla, J. Blanco-Gálvez, L. García-Rodríguez, W. Gernjak, S. Malato-Rodríguez, First experimental results of a new hybrid solar/gas multi-effect distillation system: The AQUASOL project, Desalination 220 (2008) 619–625.
[38] D.C. Alarcón-Padilla, L. García-Rodríguez, J. Blanco-Gálvez, Experimental assessment of connection of an absorption heat pump to a multi-effect distillation unit, Desalination 250 (2010) 500–505.
[39] B.N. Taylor, C.E. Kuyatt, Guidelines for evaluating and expressing the uncertainty of NIST measurement results, National Institute of Standards and Technology Technical Note 1297, 1994.
[40] A.M. El-Nashar, Predicting part load performance of small MED evaporators—A simple simulation program and its experimental verification, Desalination 130 (2000) 217–234.

[41] P. Fernández-Izquierdo, L. García-Rodríguez, D.C. Alarcón-Padilla, P. Palenzuela, I. Martín-Mateos, Experimental analysis of a multi-effect distillation unit operated out of nominal conditions, Desalination 284 (2012) 233–237.
[42] A. Jernqvist, M. Jernqvist, G. Aly, Simulation of thermal desalination processes, Desalination 134 (2001) 187–193.
[43] R.K. Kamali, A. Abbassi, S.A. Sadough Vanini, A simulation model and parametric study of MED–TVC process, Desalination 235 (2009) 340–351.
[44] D. Zhao, J. Xue, S. Li, H. Sun, Q. Zhang, Theoretical analyses of thermal and economical aspects of multi-effect distillation desalination dealing with high-salinity wastewater, Desalination 273 (2011) 292–298.